

Influence of acidity on liquid–liquid phase transitions of mixed SOA proxy–inorganic aerosol droplets

Yueling Chen¹& Xiangyu Pei¹, Huichao Liu¹, Yikan Meng¹, Zhengning Xu¹, Fei Zhang¹, Chun Xiong¹, Thomas C. Preston³, Zhibin Wang^{1,2,4*}

¹College of Environmental and Resource Sciences, Zhejiang Provincial Key Laboratory of Organic Pollution Process and Control, Zhejiang University, Hangzhou 310058, China

²ZJU-Hangzhou Global Scientific and Technological Innovation Center, Zhejiang University, Hangzhou 311215, China

³Department of Atmospheric and Oceanic Sciences and Department of Chemistry, McGill University, 805 Sherbrooke Street West, Montreal, Quebec H3A 0B9, Canada

⁴Key Laboratory of Environment Remediation and Ecological Health, Ministry of Education, Zhejiang University, Hangzhou 310058, China

Correspondence to: Zhibin Wang (wangzhibin@zju.edu.cn)

Yueling Chen and Xiangyu Pei contribute equally to this work.

Abstract. Phase state and morphology of aerosol particles play a critical role in determining their effect on climate. While aerosol acidity has been identified as a key factor affecting the multiphase chemistry and phase transitions, the impact of acidity on phase transition of multicomponent aerosol particles has not been extensively studied in situ. In this work, we employ^{ed} an aerosol optical tweezer (AOT) to probe the impact of acidity on the phase transition behavior of levitated aerosol particles. Our results reveal^{ed} that higher acidity decreases the separation relative humidity (SRH) of aerosol droplets mixed with ammonium sulfate (AS) and secondary organic aerosol (SOA) proxy, such as 3-methylglutaric acid (3-MGA), 1,2,6-hexanetriol (HEXT) and 2,5-hexanediol (HEXD) across aerosol pH in atmospheric condition. Phase separation of organic acids was more sensitive to acidity compared to organic alcohols. We found the mixing relative humidity (MRH) was consistently higher than the SRH in several systems. Phase-separating systems, including 3-MGA/AS, HEXT/AS, and HEXD/AS, exhibited oxygen-to-carbon ratios (O:C) of 0.67, 0.50, and 0.33, respectively. In contrast, liquid-liquid phase separation (LLPS) did not occur in the high O:C system of glycerol/AS, which had an O:C of 1.00. Additionally, the morphology of 42 out of the 46 aerosol particles that underwent LLPS was observed to be a core-shell. Our findings provide a comprehensive understanding of the pH-dependent LLPS in individual suspended aerosol droplets and pave the way for future research on phase separation of atmospheric aerosol particles.

1 Introduction

Atmospheric aerosol particles can directly and indirectly impact climate by absorbing and scattering light and acting as cloud condensation nuclei (Rosenfeld et al., 2014). Particle morphology is a critical factor influencing the physiochemical properties

31 of aerosols such as their optical properties, chemistry, and nucleation processes (Freedman et al., 2009; Corral Arroyo et al.,
32 2022; Cosman et al., 2008; Lam et al., 2021; Petters and Kreidenweis, 2007; Mikhailov et al., 2021). Morphology can be
33 broadly categorized into single-phase homogeneous morphology and phase separation morphology (Bertram et al. 2011;
34 Ciobanu et al. 2009), based on the phase state of the particle. For droplets with a phase separation morphology, the two main
35 equilibrium morphologies are a fully engulfed (core-shell) structure and a partially engulfed structure (Reid et al. 2011).
36 Droplets can undergo phase transition processes and thus the morphology would be changed. The composition and mass of
37 inorganic and organic components impact the phase transition characteristics of a particle. With a decrease of particle water
38 content, a transition occurs from single homogenous liquid phase to two separated liquid phases, which is known as liquid-
39 liquid phase separation (LLPS; [Freedman et al., 2017](#)). The relative humidity (RH) when the LLPS occurs is defined as
40 separation relative humidity (SRH). The reverse process, in which two liquid phases mix into a single homogenous liquid
41 phase, is referred to as liquid-liquid phase mixing and the corresponding RH is the mixing RH (MRH; You et al., 2014;
42 Gorkowski et al., 2017).

43
44 The phenomenon of LLPS has garnered considerable attention from the atmospheric research community due to its potential
45 role in affecting the physiochemical properties of atmospheric aerosols ([Kucinski et al., 2019](#); Ott et al., 2020; Freedman,
46 2020). Song et al. (2012) using optical microscopy studied the relationship between LLPS and the oxygen-to-carbon ratio
47 (O:C) and discovered that LLPS was consistently observed when $O:C < 0.56$, while it was never observed when $O:C > 0.80$.
48 For O:C between 0.56 and 0.80, the occurrence of LLPS was influenced by the types of organic functional groups. Gorkowski
49 et al. (2020) utilized experimental results of previous studies on LLPS and morphology, observing a general trend in
50 morphology from partially engulfed to core shell and finally homogeneous as oxidation increased. More recently, it is found
51 that submicrometer-sized aerosol particles had a lower SRH compared to micrometer-sized droplets (Kucinski et al., 2021;
52 Ohno et al., 2021). Meanwhile, Stewart et al. (2015) employed aerosol optical tweezer (AOT) to investigate the morphologies
53 of aqueous droplets. They found in the polyethylene glycol (PEG)/ammonium sulfate (AS) system, droplets formed
54 predominately core-shell particles when the AS content was high and partially engulfed when the PEG content was high.

55
56 One factor that could influence the phase transitions of aerosol particles is the aerosol pH. The pH values for misty cloud and
57 fog droplets generally range between 2 and 7, whereas continental and marine aerosol particles exhibit a wider range of pH
58 values, from -1 to 5 and 0 to 8, respectively (Pye et al., 2020; Angle et al., 2021; Weber et al., 2016; Tilgner et al., 2021; Zheng
59 et al., 2020). Meanwhile, aerosol pH is size-dependent, with the fine mode showing lower 1–4 pH units than the coarse mode
60 (Fang et al., 2017; Young et al., 2013; Guo et al., 2017). Losey et al. (2018) studied six organic components and discovered
61 that phase separation may be hindered by the addition of sulfuric acid, while the SRH of 3-methylglutaric acid/ammonium
62 sulfate system was found to decrease with the addition of sodium hydroxide (Losey et al. 2016), as the deprotonation of organic
63 component or difference in salting out ability of inorganic may change the SRH. More recently, Tong et al. (2022) investigated

64 the effect of acidity on phase separation in single suspended microdroplets using AOT. Their results showed that the pH can
65 affect the miscibility of the mixture and high acidity results in a reduced SRH of 1,2,6-hexanetriol.

66

67 Our aim with this work is to gain a comprehensive understanding of the influence of pH on phase transitions in suspended
68 droplets. To that end, we investigated pH-dependent SRH and MRH, as well as morphologies of aqueous droplets using AOT,
69 meanwhile discussed the effect of O:C on phase separation behavior. Compared to substrate-based measurement techniques,
70 AOT can suspend droplets without any substrate contact, providing a more realistic simulation of the behavior of aerosols in
71 the atmosphere (Wang et al., 2021; Cui et al., 2021; Redding et al., 2015; Gong et al., 2018; Rafferty et al., 2023). We measured
72 droplets containing AS and a range of organic compounds with varying O:C. ~~We discuss how o~~Our findings provide insight
73 into the mechanisms behind pH-dependent phase transitions in levitated droplets, ~~along with the~~and have implications for
74 fields such as climate science. Overall, our study highlights the importance of considering pH as a key factor in the phase
75 transition behavior of micron-sized droplets and underscores the need for further research to fully understand the complex
76 interactions between pH and phase transitions in these atmospherically relevant systems.

77 2 Methods

78 2.1 Aerosol generation

79 Four organics components: glycerol (GL), 3-methylglutaric acid (3-MGA), 1,2,6-hexanetriol (HEXT), and 2,5-hexanediol
80 (HEXD), were chosen ~~because as~~ they are commonly-used secondary organic aerosol (SOA) proxies (Lam et al., 2021;
81 Gorkowski et al., 2020). O:C of the selected chemicals varied from 1 to 0.33 (**Table 1**), which is similar to the real
82 atmospheric SOA (Canagaratna et al., 2015; Mahrt et al., 2021). AS was chosen as the inorganic salt component due to its
83 widespread occurrence in the atmospheric environment. All concentrations of organics and AS in the mother solutions were
84 50 g/L. The pure organic and inorganic components were dissolved in ultrapure water (Millipore, resistivity of 18.2 M Ω) to
85 create solutions with organic-to-inorganic mass ratio (OIR) of 1:1. The pH of studied systems were adjusted within the range
86 of 0.48 to 6.53 by using either concentrated sulfuric acid (SA) or sodium hydroxide (NaOH) solution (5.29 mol/L). Sodium
87 hydroxide, a strong base, allowed for pH adjustment with minimal usage (Losey et al., 2016). However, it is necessary to
88 acknowledge that the addition of NaOH changed~~s~~ the composition of the inorganic part of the solution, potentially affecting
89 the SRH values measured. ~~For the 3-MGA/AS system, either SA or NaOH was utilized, while for the HEXT/AS and HEXD/AS~~
90 ~~systems, only SA was used.~~The pH of each solution was measured using a pH meter (Mettler Toledo Instruments Co., Ltd.,
91 Shanghai, China). The purity and supplier of the compounds used in this study ~~were arc~~ summarized in **Table S1**.

92

Table 1. Information of the solutions used to generate aerosol droplets.

Solution ID	Organic component	O:C ratio	pH
GL	glycerol	1.00	5.24±0.01
3-MGA-I	3-methylglutaric acid	0.67	0.48±0.01
3-MGA-II			1.19±0.01
3-MGA-III			2.70±0.01
3-MGA-IV			3.70±0.01
3-MGA-V			5.21±0.02
3-MGA-VI			6.53±0.02
HEXT-I	1,2,6-hexanetriol	0.50	0.92±0.01
HEXT-II			2.02±0.01
HEXT-III			3.14±0.01
HEXT-IV			5.11±0.02
HEXD-I	2,5-hexanediol	0.33	1.39±0.01
HEXD-II			2.03±0.01
HEXD-III			2.71±0.01
HEXD-IV			3.13±0.01
HEXD-V			5.01±0.01

94

95 2.2 Experimental setup

96 A schematic illustration of the experimental setup is presented in **Fig. S1**. The aerosol optical tweezer system consists of a
97 custom-made levitation chamber that integrates the optical trapping system, the illumination and imaging system, and the
98 aerosol generation system. A 532 nm (Opus 532-2W) laser was used to create an optical trap with a 100x oil immersion
99 objective (Olympus, UPLFLN100XO, NA 1.30) pressed against a glass coverslip (Nest, thickness 160-190 μm). The
100 illumination and imaging system includes a 450 nm LED (Daheng Optics, GCI060404) and a camera (Thorlabs, CS165CU/M)
101 to illuminate and image the particle. Two low pass filters (Andover, 500FL07-25) were used in front of the camera lens to
102 remove the influence of back scattered light of the 532 nm laser to photograph clear image of the particle. The Raman scattered
103 light passed through two 50:50 beam splitters (CVI Laser Optics, BTF-VIS-50-2501M-C) and a notch filter (Semrock, NFD01-
104 532-25x36) and was focused into the Raman spectrograph. A spectrograph (ZOLIX, Omni-λ5004i) ~~is~~was used to measure the
105 Stokes shifted Raman spectrum. A 20 μm entrance slit width and 1200 groove/mm diffraction grating with a blaze wavelength
106 of 500 nm were used to achieve a spectral resolution of 0.021 nm. The wavelength position of spectrograph was calibrated
107 with an Hg-laser. The Raman scattered light was recorded every 4 seconds s with range of 624.24-665.40 nm.

108

109 As droplets are introduced continuously into the chamber from a medical nebulizer (LANDWIND, PN100), smaller droplets
110 undergo a process of collision and coalescence, leading to the formation of larger droplets that can be readily trapped near the
111 focal point of the laser. In most cases, droplets can be successfully captured within 30 s after the introduction of an aerosol
112 plume into the cell. Air with relative humidity (RH) of 100% and 0% were mixed to produce wet air with a desired RH. The
113 flow rates of the humidified and dry air streams were regulated by mass flow controllers (MFCs, Tianjin Gastool Instruments
114 Co., Ltd., Tianjin, China, GT130D), with a combined flow rate of 0.3 L/min in total. Two humidity sensors (Sensirion, SHT85)
115 were utilized, with a precision of $\pm 1.5\%$. Since the sensor located behind the chamber was positioned in close proximity (~ 80
116 mm) to the droplet, its observed values were used as a surrogate for measuring the RH inside the chamber. The RH values
117 were reduced in increments of 5% every 30 minutes (Tong et al., 2022; Stewart et al., 2015) until droplet phase separation
118 occurred. The measured values of RH given by the sensors were used as the phase separation RH. Subsequently, the RH level
119 was set to 100%, to investigate the phase mixing of the droplets. The entire experiment was repeated ~~2~~4 times for each
120 system.

121 2.3 Determination of phase transitions

122 When a transparent or weakly absorbing spherical particle is trapped, it can behave as a high-quality factor optical cavity that
123 supports sharp optical resonances, resulting in cavity-enhanced Raman scattering. These resonances can be observed as peaks
124 in the Raman spectrum of a particle and are often referred to as whispering gallery modes (WGMs). In principle, particle
125 morphology can be deduced from the WGMs, as inhomogeneities in the refractive index can disrupt the circulation of the
126 WGMs (Lin et al., 1992; Mitchem et al., 2006). Raman spectra measurements of single droplets in various morphological
127 states are presented in **Figure 1**. When the droplet was in a homogeneous phase morphology, the droplet acted as a high-
128 quality microcavity and sharp WGM peaks overlapped with the spontaneous Raman spectrum (**Fig. 1a**). When the droplet was
129 in a state of a core-shell structure, observed WGMs were clearly diminished in measured spectra (**Fig. 1b**). The origin of the
130 damping of the WGMs is the radial homogeneity that is present when the particle is separated into a hydrophilic core and a
131 hydrophobic shell. As a result, when fitting the Raman spectra with the Mie scattering model for homogeneous droplets, the
132 error in the best-fits greatly increase. Examination of the retrieved radius and refractive index reveals a clear break with fits
133 for that of a homogeneous sphere. Therefore, the point at which a significant break in particle size and refractive index occurred
134 can be used as the point at which core-shell phase separation occurs. As illustrated in **Fig. 1c**, when the droplet was partially-
135 engulfed and non-spherical, WGM peaks in the spectrum ~~are~~were absent (Reid et al., 2011). The origin of the spontaneous
136 Raman peaks at 3300 cm^{-1} and $\sim 3050\text{ cm}^{-1}$ are identified as the spurious or weakened WGM peaks and the vibration of N-H
137 bond, respectively. Overall, the results of this analysis demonstrate the dynamic changes in the Raman spectra of single droplets
138 as they undergo morphological transitions (Sullivan et al., 2020; Stewart et al., 2015; Tong et al., 2022).

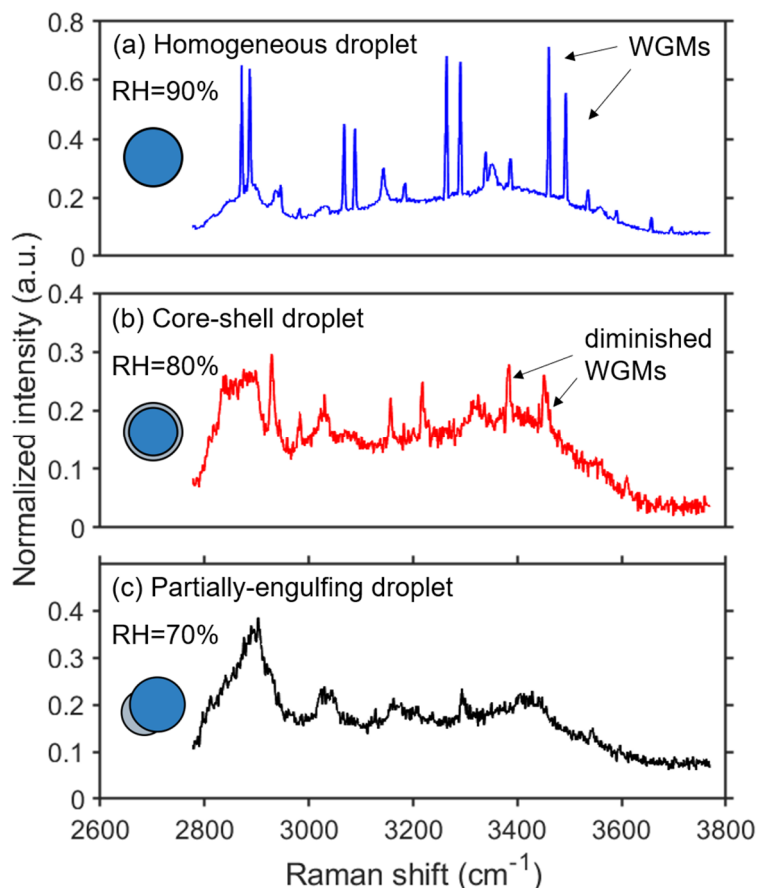


Figure 1. Raman spectra of 3-MGA-II microdroplets: (a) a homogenous droplet (RH = 90%); (b) a core-shell droplet (RH = 80%); (c) a partially-engulfed droplet (RH=70%). The WGMs are marked by black arrows. The normalization of the peak is achieved by dividing it by the maximum value of the spectrum's intensity, respectively.

The peak finding method used in this study is based on the ipeak code developed by O'Haver (2022). In short, the code first smooths the first derivative of the signal and identified downward-going zero-crossings that met a certain predetermined minimum slope and amplitude threshold. By adjusting the corresponding parameters, it is possible to accurately detect the desired peaks. The algorithm used to fit WGM peaks in spectra from homogenous spheres in this study was proposed by Preston and Reid (2013) and Preston and Reid (2015). The algorithm compares observed peak positions to expected positions calculated using a resonance condition from Mie theory. Error is minimized by varying particle size and refractive index (i.e. the parameters of best-fit). The method has been demonstrated to provide a rapid determination of the fitted radius and refractive index with an accuracy of ± 2 nm and ± 0.0005 , respectively. During the experiment with reduced RH, we had to adjust the laser power to ensure the stable capture of droplets, which will affect the peak intensity. To eliminate this effect, as

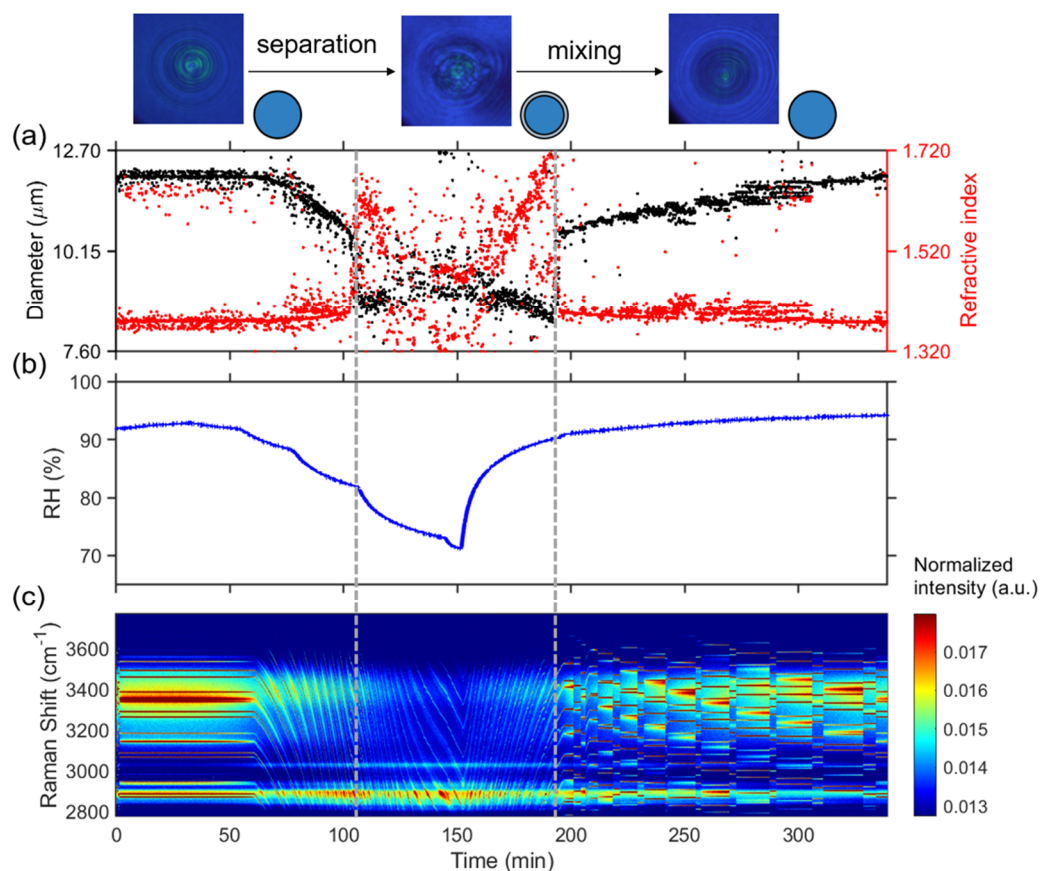
153 demonstrated by Tong et al. (2022), we normalized all Raman spectra used in this study by the area below the spontaneous
154 Raman signals.

155 **3 Results and discussion**

156 **3.1 Phase behaviors of droplets mixed SOA proxy with AS**

157 **Fig. 2** presents the results of time-resolved Raman spectra of aerosol droplets produced from a 3-MGA-II solution under
158 continuously varying RH, as well as the corresponding particle size and refractive index values. To enable temperature and
159 RH to stabilize, the chamber was conditioned with airflow for 50 minutes after trapping a particle. During the dehumidification
160 process, the particle diameter decreased from 11.85 μm to 9.03 μm and the refractive index increased from 1.379 to 1.475
161 when RH decreased from 93.0% to 70.0%. The particle size and water content decreased with RH due to the equilibrium
162 partitioning of water molecules between vapor and droplets. Meanwhile, the refractive index of the droplets gradually increased
163 as the water content decreases. When LLPS occurred, the droplets changed from a symmetrical homogeneous phase to either
164 an asymmetrical partially engulfed structure which led to the disappearance of the WGMs, or the formation of a core-shell
165 structure. As RH in the reaction chamber was reduced, the LLPS was initiated, marked by the variations of the WGM signal
166 (See **Fig. 1b**). This was achieved by reducing setting RH (setting values) by 5% at 30-minute intervals until the organic phase
167 separated from the water-rich phase and then continuing decreasing RH by 10%-15%. **Fig. 2a** illustrates how the fitting of the
168 droplet diameter and the refractive index deteriorated as the shell develops, indicating phase separation. The refractive index's
169 shift results from a significant change in the radial profile due to the formation of a core-shell structure. Additionally, the
170 persistence of strong WGMs indicates that the morphology of the droplet remains spherical following LLPS and is core-shell.
171 During the RH increased from 70% to 95%, the reappearance of the continuously shifting WGM signal ~~was is~~-observed,
172 suggesting that the inorganic phase has mixed with the organic phase, and droplet returned to a homogeneous phase. During
173 the humidification process, there is an opposite trend observed in the particle size and refractive index of the droplet compared
174 to the dehumidification process. In conclusion, the variations of the WGM signal can serve as a reliable indicator of the
175 occurrence of liquid-liquid phase separation or mixing, and the RH at these points can be considered as the SRH or MRH,
176 respectively. The observed phase transitions of droplets produced from HEXT-IV and HEXD-V solutions ~~were-are~~ shown in
177 **Fig. 3** and **Fig. 4** respectively.

178



179

180

181

182

183

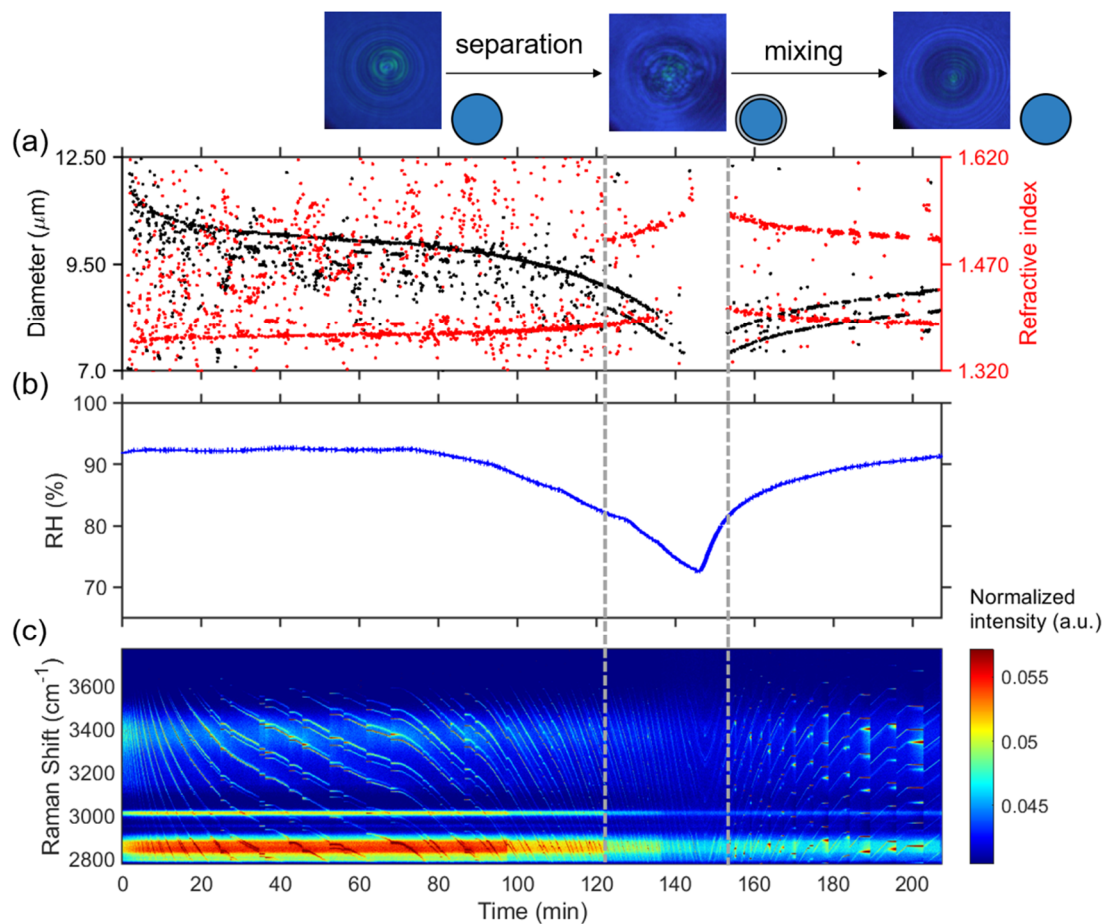
184

185

186

187

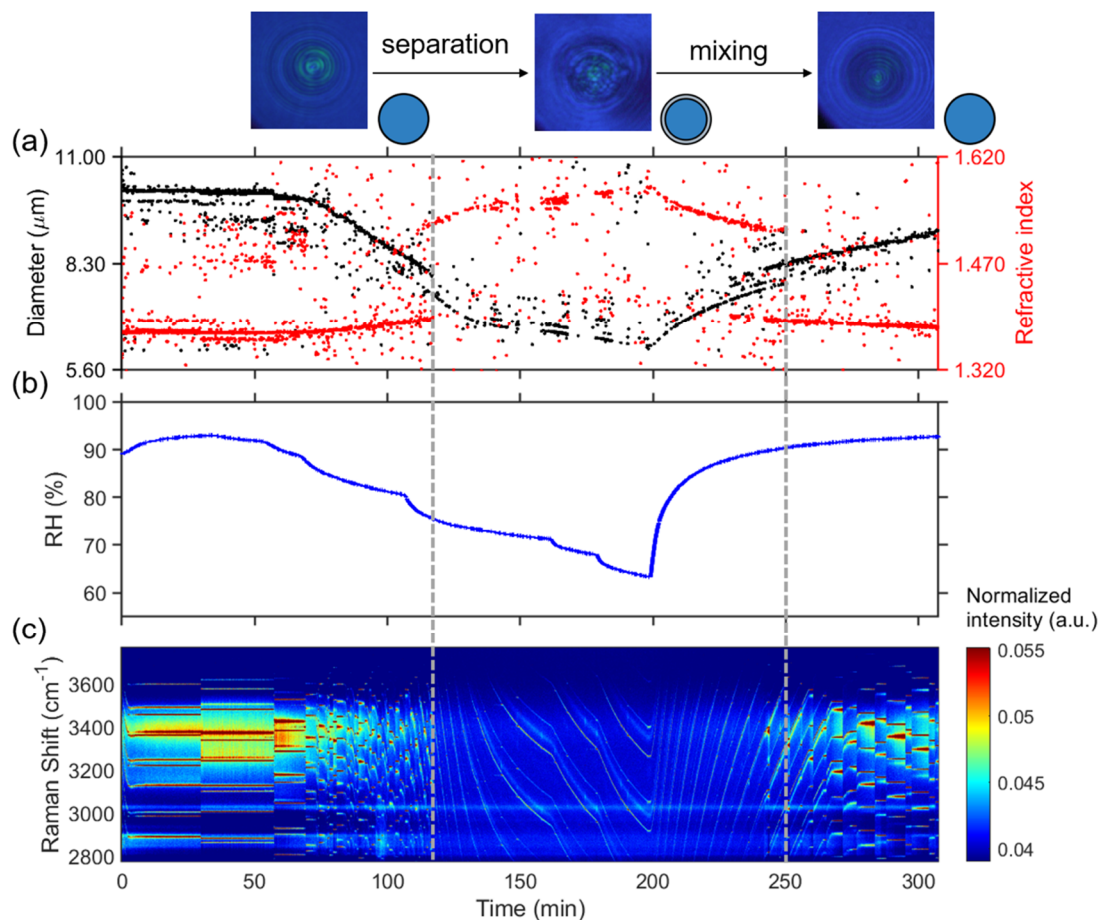
Figure 2. Liquid-liquid phase separation and mixing of aqueous 3-MGA-II. Schematic diagram of phase states is on the top of the figure. (a) Timescale of changes in droplet size and refractive index, determined from fitting the Raman shift positions of the WGMs. (b) RH variation after the trapping chamber during the humidity changing process. (c) Time-resolved Raman spectra. The cessation of the random motion of inclusions within the droplet and the resultant formation of a core-shell structure are indicated by the grey dashed line on the left. The grey dashed line on the right serves as an indication of the point at which the droplet morphology transitioned from a state of separated phases to a homogeneous phase. The Raman spectra at 53 min, 113 min, 130 min are shown in **Fig. 1(a), (b), (c)**, respectively. Fitting errors of the WGMs were presented in **Fig. S3**.



188

189 **Figure 3.** Liquid-liquid phase separation of aqueous of HEXT-IV. (a) Timescale of changes in droplet size and refractive index,
 190 determined from fitting the Raman shift positions of the WGMs. (b) RH variation after the trapping chamber during the
 191 humidity changing process with time. (c) Time-resolved Raman spectra. The cessation of the random motion of inclusions
 192 within the droplet and the resultant formation of a core-shell structure are indicated by the grey dashed line on the left. The
 193 grey dashed line on the right serves as an indication of the point at which the droplet morphology transitions from a state of
 194 phase separation to a homogeneous phase morphology. This transformation is characterized by the occurrence of phase mixing.

195



196

197 **Figure 4.** Liquid-liquid phase separation of aqueous of HEXD-V. (a) Timescale of changes in droplet size and refractive index,
 198 determined from fitting the Raman shift positions of the WGMs. (b) RH variation after the trapping chamber during the
 199 humidity changing process. (c) Time-resolved Raman spectra. The cessation of the random motion of inclusions within the
 200 droplet and the resultant formation of a core-shell structure are indicated by the grey dashed line on the left. The grey dashed
 201 line on the right serves as an indication of the point at which the droplet morphology transitions from a state of phase separation
 202 to a homogeneous phase morphology. This transformation is characterized by the occurrence of phase mixing.

203

204 **Fig. S2** presents the results of time-resolved Raman spectra of aerosol droplets produced from GL/AS solution under
 205 continuously varying RH, as well as the corresponding particle diameter and refractive index values. At the start of the
 206 experiment, the chamber RH was held at 93% for approximately 75 minutes. The spectrum during this period revealed a clear
 207 bright trend, indicative of the presence of many WGMs in the newly captured droplets. As the chamber RH dropped to a
 208 minimum value of 71.5% at around 200 minutes, the position of the WGMs in each spectral snapshot shifted continuously,
 209 following the same trend as the chamber RH. This observation suggests that the droplet was homogeneous and that no phase

210 separation occurred in the experimental RH range. The phenomenon regarding the GL/AS system is consistent with the
211 conclusion by Song et al. (2013) and Gorkowski et al. (2020).

212 3.2 Effect of pH on SRH and MRH of different systems

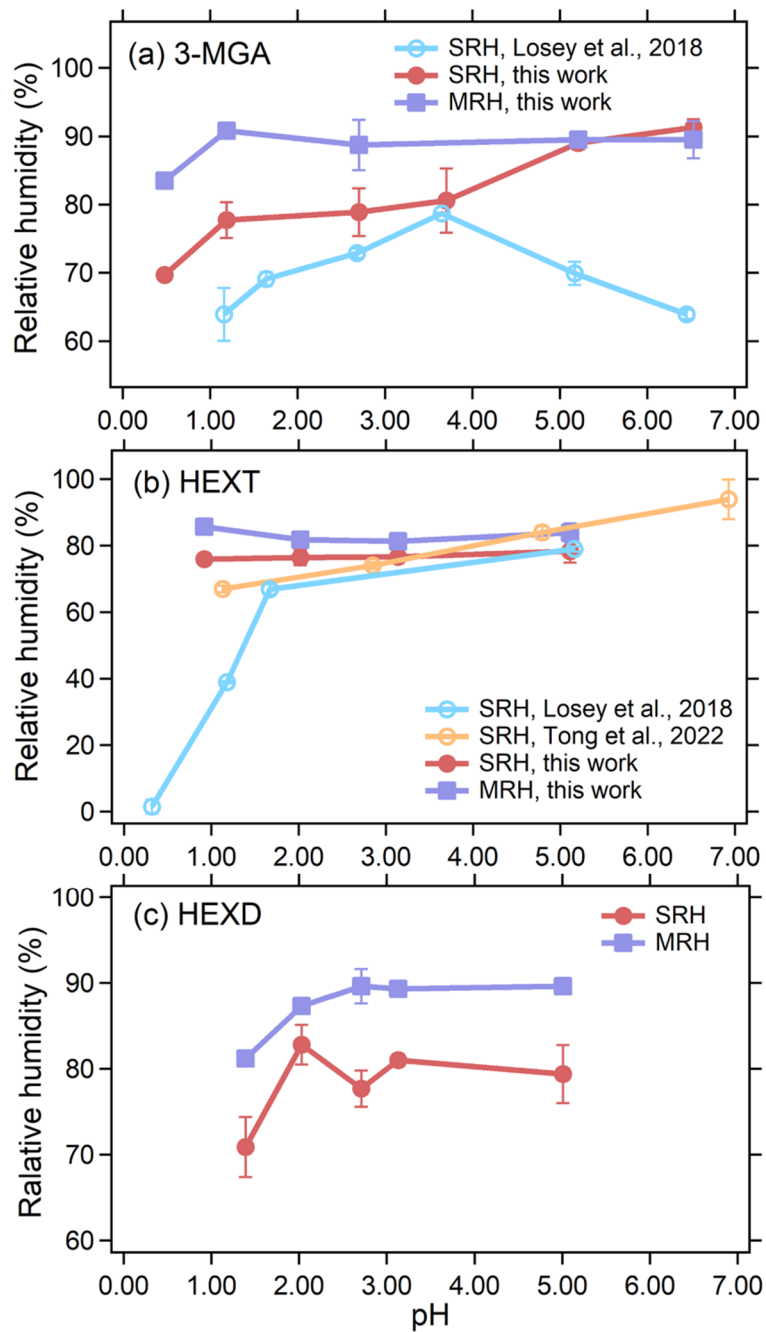
213 The SRH and MRH of aerosol droplets produced from 3-MGA-I~VI solution are shown in Fig. 5a and Table S2. The pH of
214 the 3-MGA/AS solution without the addition of an acid or base was 2.70. For solutions with a lower pH (1.19 and 0.48), SA
215 was added, while NaOH was added to solutions with a higher pH (3.70, 5.21, and 6.53) to adjust their pH levels. The SRH
216 values were 92.7%, 89.5%, 80.6%, 79.7%, 76.2% and 69.7% at pH of 6.53, 5.21, 3.70, 2.70, 1.19 and 0.48, respectively. It is
217 worth mentioning that when the pH of the 3-MGA system is 0.48, only two sets of valid parallel experimental data are available,
218 even though we had repeated the experiment several times. Because in other parallel experiments, the SRH of the droplet is
219 lower than the capture range of AOT, the AOT would not be able to continue the capture when the particle size decreases to
220 ~6 μm . Therefore, the actual SRH may be a bit lower at this pH, but this does not affect the results we discuss later. With a
221 decrease in pH, ammonium sulfate transforms into ammonium bisulfate. Our results are consistent with the hypothesis that
222 Predicted by the Hofmeister series, ammonium bisulfate exhibits a weaker salting out effect compared to ammonium sulfate
223 and thus hinders the ability of organic matter to precipitate out of the solution (Losey et al., 2018). The MRH values at pH
224 6.53, 5.21, 2.70, 1.19 and 0.48 were 87.6%, 89.5%, 87.3%, 83.9% and 83.5%, respectively, and are generally higher than
225 corresponding SRH, especially in the low pH range (<5.00). The SRH was higher than the MRH at pH 6.53, which was
226 abnormal because a lower SRH is commonly expected due to the activation barrier. We do not have a specific explanation for
227 this phenomenon, while it should be noted that the observed values were relatively close to each other, indicating that the
228 higher SRH at pH 6.53 might potentially be attributed to experimental error. The hysteresis between SRH and MRH existed
229 because the SRH process has an activation barrier while the MRH process does not, and lower RH is needed for the aerosol
230 droplet to overcome the activation barrier to form two phases (Freedman, 2020). Similar results were also observed in
231 HEXT/AS and HEXD/AS systems. Additionally, the pH-dependent SRHs obtained in this study were compared to those
232 reported by Losey et al. (2018), as depicted in Fig. 5a. It is worth mentioned that the solute concentration used in our study
233 (50g/L) is comparable to Losey et al. (2018) (5.0 wt%), allowing for meaningful comparison of results. Overall, the SRHs of
234 3-MGA obtained in this study was higher than the results of Losey et al. (2018). When the pH was lower than 3.70, in 3-MGA
235 system, the present study followed a similar trend as the results of Losey et al. (2018), with the SRH decreasing as the pH
236 decreased. However, when the pH was greater than 3.70, our study showed an opposite trend compared to the results of Losey
237 et al. (2018). The observed discrepancy may be attributed to the distinct ambient conditions of the droplets. The laser levitation,
238 resulting in a spherical morphology, while the optical microscopy involves substrate deposition, leading to a morphology
239 resembling a spherical crown (Tong et al., 2022; Zhou et al., 2014). The underlying reasons for these differences are currently
240 unclear, and further investigations are needed.

241

242 In addition to 3-MGA, we also studied two organic/AS systems to investigate how acidity affects SRH and MRH of aerosols
243 of differing composition. These results are shown in **Fig. 5** and tabulated in **Table 2**. The separation diameter (SD) of 3-
244 MGA/AS ranges from 7.23 μm to 9.74 μm , with a corresponding separation refractive index (SRI) ranging from 1.362 to 1.515.
245 For HEXT/AS, the SD ranges from 9.01 μm to 9.90 μm , while the SRI ranges from 1.396 to 1.421. Lastly, the SD of HEXD/AS
246 ranges from 7.45 μm to 8.97 μm , with the SRI ranging from 1.382 to 1.406. The data suggests that acidity did not have a
247 noticeable effect on the MRH of the various systems. The pH of the HEXT/AS solution without the addition of any acid was
248 5.11, and ~~sulfuric acid~~SA was utilized to adjust the pH to lower levels (3.14, 2.02 and 0.92). The SRH values of HEXT/AS
249 system (O:C=0.50) decreased as the pH decreased, with values of 78.3%, 76.6%, 76.4% and 75.7% at pH values of 5.11, 3.14,
250 2.02 and 0.92, respectively. The trend is similar to the 3-MGA (O:C=0.67) system, and the reason why SRH decreased may
251 be due to the acid enhancing the miscibility of organic alcohols and inorganic substances, resulting in a greater difficulty in
252 separating the hydrophobic phase from the water-rich phase (Tong et al., 2022). Still, we observed SRH was not strongly
253 dependent on pH for HEXT/AS, compared to 3-MGA/AS system. This is likely due to the fact that organic alcohols have a
254 large pK_a (e.g. the pK_a of HEXT is 14.3) and therefore exhibit minimal ionization in the pH range studied here (Wade and
255 Simek, 2020). Additionally, the relative molecular interactions between alcohols and water are weaker than those of acids,
256 leading to a weaker dependence of salting out ability of AS in the HEXT/AS system. The results of Losey et al. (2018) and
257 Tong et al. (2022) were also depicted in **Fig. 5b**. Our results differ from those of Losey et al. (2018), who observed a significant
258 decline in SRH as the pH decreased. The specific reason for the discrepancy remains unclear, but we speculate it may due to
259 different condition of droplet. ~~Moreover, the concentration of HEXT in this work (50g/L) is higher than concentration (2.5~~
260 ~~wt%, about 26 g/L) of Losey et al. (2018). The higher concentration may enhance the precipitation of organic matter from the~~
261 ~~inorganic salts in our work.~~ In contrast to the findings of Tong et al. (2022), our study observed a less pronounced trend in the
262 values of SRH, and a narrower range in the distribution of SRH compared to literature values. The difference in OIR between
263 this study (1:1) and Tong et al. (2022) (2:1) may account for the discrepancy in SRH. Previous studies (Ma et al., 2021; Stewart
264 et al., 2015; Song et al., 2012) indicated that OIR differences could affect SRH, but SRH was not significantly dependent on
265 OIR. The discrepancy in SRH may also be due to the variations in experimental conditions, such as laser power, experimental
266 duration, etc. For HEXD/AS (O:C=0.33) system, the pH of the HEXD/AS solution without the addition of any acid was 5.01,
267 and SA was used to adjust the pH to lower levels (3.13, 2.71, 2.03 and 1.39). SRH decreased significantly when the pH ~~is~~
268 was less than 2.00, while acidity had no significant effect on SRH when pH is greater than 2.00, with values of 79.4%, 81.0%,
269 77.7%, 82.8% and 70.9% at pH values of 5.01, 3.13, 2.71, 2.03 and 1.39, respectively. This phenomenon was attributed to a
270 mechanism similar to that observed in HEXT/AS. To our knowledge, this is the first investigation on the pH-dependent phase
271 transition of HEXD/AS at the single particle level in a contact-free environment.

272
273 The pH values of misty cloud and fog droplets typically fall within the range of 2 to 7, whereas continental and marine aerosol
274 particles display a broader spectrum of pH values (Pye et al., 2020; Tilgner et al., 2021). Our research suggests that in real

275 atmospheric conditions, phase separation behavior of droplets may be influenced significantly by their acidity. It is challenging
276 to measure the droplet pH of the investigated system using AOT. However, previous studies (Coddens et al., 2019; Li et al.,
277 2023) have shown that at high RH (90%~~---~~100%), the difference in the pH values between droplets and bulk solution is
278 relatively small. Therefore, we used bulk solution pH as an indicator of pH at droplet phase transition. This study focused on
279 volatile organics and was conducted over a relatively long period, which may have affected our results. Nevertheless, the
280 organic compounds used in this study have low volatility. For instance, the vapor pressure of 3-MGA is 7.41×10^{-7} to $2.92 \times 10^{-}$
281 4 mmHg (DTXSID50871000, United States Environmental Protection Agency), compare to normal volatile organic
282 components of atmospheric aerosol, such as 2-Methyl-1-propanol with vapor pressure of 10.5 to 16.4 mmHg
283 (DTXSID0021759, United States Environmental Protection Agency). Volatility information of other organics are provided in
284 the Table S5. Also, the influence of droplet size change in our system can be neglected. For example, as shown in **Fig. 2**, the
285 droplet size ~~is~~was basically same at the beginning and the end of the experiment at the same RH 93.0% (11.85 μm at the
286 beginning and 11.79 μm at the end).



288

289 **Figure 5.** SRHs and MRHs as a function of pH for (a) 3-MGA/AS system, (b) HEXT/AS system, (c) HEXD/AS system.

290 Hollow circles represent data from Losey et al. (2018) and Tong et al. (2022). The error bars of SRHs and MRHs are derived

291 from multiple measurements.

292 **Table 2.** SRH information for each pH studied as well as initial diameter, separation diameter (SD), separation refractive index
 293 (SRI), MRH, mixing diameter (MD), and mixing refractive index (MRI) data.

3-MGA/AS system (O:C=0.67)							
Initial pH	Initial Diameter(μm)	SRH (%)	SD (μm)	SRI ($\lambda=650$ nm)	MRH (%)	MD (μm)	MRI ($\lambda=650$ nm)
0.48	10.97 \pm 1.57	69.7 \pm 0.2	7.23 \pm 1.72	1.515 \pm 0.086	83.5	6.82	1.540
1.19	11.23 \pm 1.20	77.7 \pm 2.6	8.68 \pm 2.38	1.454 \pm 0.100	90.8 \pm 0.2	9.08 \pm 1.64	1.394 \pm 0.009
2.70	12.02 \pm 2.94	78.9 \pm 3.5	7.88 \pm 1.21	1.493 \pm 0.082	88.7 \pm 3.7	6.81 \pm 2.76	1.506 \pm 0.094
3.70	10.87 \pm 1.87	80.6 \pm 4.7	7.24 \pm 1.00	1.491 \pm 0.088			
5.21	11.06 \pm 1.63	89.0 \pm 0.9	8.93 \pm 0.16	1.362 \pm 0.014	89.5	7.89	1.381
6.53	13.73 \pm 0.41	91.3 \pm 1.2	9.74 \pm 0.36	1.444 \pm 0.187	89.5 \pm 2.7	7.89 \pm 0.06	1.383 \pm 0.01
HEXT/AS system (O:C=0.50)							
0.92	13.52 \pm 1.6	75.9 \pm 0.2	9.90 \pm 0.76	1.421 \pm 0.017	85.7	10.83	1.420
2.02	12.88 \pm 1.0	76.4 \pm 2.3	9.09 \pm 0.46	1.409 \pm 0.007	81.8	9.34	1.410
3.14	12.31 \pm 0.8	76.6 \pm 1.5	9.01 \pm 0.47	1.408 \pm 0.002	81.3	9.04	1.409
5.11	13.53 \pm 0.4	78.3 \pm 3.4	9.15 \pm 0.35	1.396 \pm 0.014	83.9 \pm 2.8	9.04 \pm 0.73	1.412
HEXD/AS system (O:C=0.33)							
1.39	11.48 \pm 0.78	70.9 \pm 3.5	7.45 \pm 0.77	1.406 \pm 0.008	81.2	7.93	1.406
2.03	10.54 \pm 0.57	82.8 \pm 2.3	7.90 \pm 0.99	1.382 \pm 0.007	87.3	8.83	1.392
2.71	14.55 \pm 1.36	77.7 \pm 2.1	8.30 \pm 0.28	1.391 \pm 0.009	89.6 \pm 2.0	8.53 \pm 0.32	1.388 \pm 0.010
3.13	11.02 \pm 0.62	81.0 \pm 0.7	8.97 \pm 0.22	1.384 \pm 0.016	89.3	9.14	1.384
5.01	12.22 \pm 2.73	79.4 \pm 3.4	8.33 \pm 0.40	1.384 \pm 0.019	89.6 \pm 0.1	8.38 \pm 0.54	1.390 \pm 0.004

294

295 3.3 Effect of O:C on phase separation behavior in different systems

296 Our findings provide evidence that phase separation of droplets persists even when the organic-inorganic system is adjusted
 297 to a specific level of acidity. An important determinant of whether droplets undergo phase separation is the O:C. To illustrate
 298 this, we have included a plot in **Fig. S4**, which show cases the experimental system used in our study alongside relevant
 299 literature values. One point that needs to be declared is **Fig. S4** only plotted for systems with no additional H₂SO₄ or NaOH.
 300 As shown in **Fig. S4**, our findings, as well as those from previous studies (You et al., 2013; O'Brien et al., 2015), indicated
 301 that there is no correlation between the occurrence of LLPS and the hydrogen-to-carbon (H:C) ratios of the organics, which is
 302 consistent with results in previous findings (Bertram et al., 2011; Song et al., 2012). However, a clear trend was observed
 303 between LLPS occurrence and the O:C of the organic components. We observed that droplets of 3-MGA/AS, HEXT/AS and
 304 HEXD/AS systems with O:C between 0.33 and 0.67 undergo LLPS. With the decrease of water content in the droplets, two
 305 distinct phases were formed: an organic-rich phase and a salt-rich aqueous phase, under both acidic and neutral conditions. By
 306 contrast, no LLPS occurred in the GL/AS system, as shown in **Fig. S2**. In general, particles with low O:C are more prone to

307 undergo LLPS. This observation is consistent with the findings of Song et al. (2012) who reported that LLPS was never
308 observed when O:C > 0.80 and always observed when O:C < 0.56.

309
310 As shown in **Fig. 2** and **Table S2**, for most spectra, WGMs remained after LLPS occurred for droplets of 3-MGA/AS. This
311 phenomenon indicates that the droplets undergo LLPS with a core-shell morphology in most conditions, which is consistent
312 with the prediction of Gorkowski et al. (2020). Meanwhile, morphology of phase-separated droplets containing either HEXT
313 or HEXD were also core-shell shape mostly, as depicted in **Fig. 3/4** and **Table S3/S4**. It is attributed to the lower interfacial
314 tension observed at higher O:C, leading to higher possibility condition for forming core-shell shaped droplets (Gorkowski et
315 al., 2020). These findings support the idea that the O:C plays a crucial role in determining the morphology of phase-separated
316 particles in organic/inorganic mixed aerosols.

317 **4 Conclusion**

318 The aim of this study ~~was~~ was to investigate the effect of pH and O:C on phase transition behavior of levitated particles using the
319 AOT. Our results show that across aerosol pH in atmospheric condition, the presence of sulfuric acid inhibited the LLPS of
320 aerosol droplets that contained organics (3-MGA, HEXT, HEXD) and AS. Additionally, the MRHs were found to be higher
321 than the SRHs. The O:C of phase-separating systems is 0.67, 0.50, 0.33, and by contrast, LLPS of the high O:C system (GL,
322 O:C=1.00) did not occur. Meanwhile, the morphology of levitated aerosol particles was studied and we found that 42 out of
323 46 droplets that underwent LLPS for a core-shell structure. The SRH of all experimental systems ranged from ~70% to 90%.
324 In certain cases, as the RH decreased, the droplet morphology changed from core-shell to partially engulfed, similar to the
325 findings reported by Kucinski et al. (2020). However, as the RH further decreased, the droplet particle size became smaller
326 than 6 μm , making it impossible to capture them using AOT. Consequently, in most instances, we were unable to observe the
327 droplet morphology at RH levels below 70%. The results presented here provide new insights into the behavior of different
328 types of aerosol droplets, and the findings have important implications for our understanding of physical and chemical
329 processes that occur in the atmosphere. It is anticipated that future studies will be carried out to examine the OIR-dependent
330 phase separation in real acidified ambient aerosols. Such research will provide insights into the morphological characteristics
331 of real aerosols and the ways in which these characteristics influence important properties such as hygroscopicity and
332 homogenous chemistry. Such information will be helpful in furthering our understanding of the impacts of ambient aerosols
333 on the environment and human health.

334
335 Additionally, in-situ pH measurement or pH estimation methods, such as the real-time AOT analysis in microdroplets reported
336 by Boyer et al. (2020) could be combined with SRH measurements for a more accurate and comprehensive analysis.

337 Furthermore, our study used a surrogate for SOA instead of in situ measurements of real SOA, which can be addressed in
338 future work using SOA generated from a smog chamber or real SOA precursors and oxidized species.

339
340 **Data availability.** The data used in this paper can be obtained from the corresponding author upon request.

341 **Author contributions.** YC built the instrument, performed the experiments, analyzed the data, plotted the figures, and wrote
342 the original draft. XP conceptualized the study, contributed to instrumentation, data analysis, discussion, and reviewed the
343 manuscript. HL and CX contributed to the instrumentation and discussion. YM contributed to the experiments and discussion.
344 ZX, FZ contributed to the discussion and manuscript review. TCP contributed to data analysis and manuscript review. ZW
345 administrated the project, conceptualized the study, reviewed the manuscript, and contributed to funding acquisition.

346 **Competing interests.** The contact author has declared that none of the authors has any competing interests.

347 **Disclaimer.** Publisher's note: Copernicus Publications remains neutral with regard to jurisdictional claims in published maps
348 and institutional affiliations.

349 **Financial support.** This research has been supported by the National Natural Science Foundation of China (grant nos.
350 91844301, 42005087, and 42005086), Key Research and Development Program of Zhejiang Province (grant nos. 2021C03165,
351 2022C03084), and the Fundamental Research Funds for the Central Universities (grant no. 2018QNA6008).

352 References

- 353 Angle, K. J., Crocker, D. R., Simpson, R. M. C., Mayer, K. J., Garofalo, L. A., Moore, A. N., Mora Garcia, S. L., Or, V. W.,
354 Srinivasan, S., Farhan, M., Sauer, J. S., Lee, C., Pothier, M. A., Farmer, D. K., Martz, T. R., Bertram, T. H., Cappa, C.
355 D., Prather, K. A., and Grassian, V. H.: Acidity across the interface from the ocean surface to sea spray aerosol, *Proc.*
356 *Natl. Acad. Sci. U.S.A.*, 118, e2018397118, <https://doi.org/10.1073/pnas.2018397118>, 2021.
- 357 Bertram, A. K., Martin, S. T., Hanna, S. J., Smith, M. L., Bodsworth, A., Chen, Q., Kuwata, M., Liu, A., You, Y., and Zorn,
358 S. R.: Predicting the relative humidities of liquid-liquid phase separation, efflorescence, and deliquescence of mixed
359 particles of ammonium sulfate, organic material, and water using the organic-to-sulfate mass ratio of the particle and the
360 oxygen-to-carbon elemental ratio of the organic component, *Atmos. Chem. Phys.*, 11, 10995-11006,
361 <https://doi.org/10.5194/acp-11-10995-2011>, 2011.
- 362 Boyer, H. C., Gorkowski, K., and Sullivan, R. C.: In situ pH measurements of individual levitated microdroplets using aerosol
363 optical tweezers, *Anal. Chem.*, 92, 1089-1096, <https://doi.org/10.1021/acs.analchem.9b04152>, 2020.
- 364 Canagaratna, M. R., Jimenez, J. L., Kroll, J. H., Chen, Q., Kessler, S. H., Massoli, P., Hildebrandt Ruiz, L., Fortner, E.,
365 Williams, L. R., Wilson, K. R., Surratt, J. D., Donahue, N. M., Jayne, J. T., and Worsnop, D. R.: Elemental ratio
366 measurements of organic compounds using aerosol mass spectrometry: characterization, improved calibration, and
367 implications, *Atmos. Chem. Phys.*, 15, 253-272, <https://doi.org/10.5194/acp-15-253-2015>, 2015.
- 368 Ciobanu, V. G.; Marcolli, C.; Krieger, U. K.; Weers, U.; Peter, T. Liquid-Liquid Phase Separation in Mixed Organic/Inorganic
369 Aerosol Particles. *J. Phys. Chem. A* 2009, 113 (41), 10966–10978.
- 370 Coddens, E. M., Angle, K. J., and Grassian, V. H.: Titration of aerosol pH through droplet coalescence, *J. Phys. Chem. Lett.*,
371 10, 4476-4483, <https://doi.org/10.1021/acs.jpcclett.9b00757>, 2019.
- 372 Corral Arroyo, P., David, G., Alpert, P. A., Parmentier, E. A., Ammann, M., and Signorell, R.: Amplification of light within
373 aerosol particles accelerates in-particle photochemistry, *Science*, 376, 293-296, <https://doi.org/10.1126/science.abm7915>,
374 2022.

375 Cosman, L. M., Knopf, D. A., and Bertram, A. K.: N₂O₅ reactive uptake on aqueous sulfuric acid solutions coated with
376 branched and straight-chain insoluble organic surfactants, *J. Phys. Chem. A*, 112, 2386, <https://doi.org/10.1021/jp710685r>,
377 2008.

378 Cui, X., Tang, M., Wang, M., and Zhu, T.: Water as a probe for pH measurement in individual particles using micro-Raman
379 spectroscopy, *Anal. Chim. Acta.*, 1186, 339089, <https://doi.org/10.1016/j.aca.2021.339089>, 2021.

380 Fang, T., Guo, H., Zeng, L., Verma, V., Nenes, A., and Weber, R. J.: Highly acidic ambient particles, soluble metals, and
381 oxidative potential: a link between sulfate and aerosol toxicity, *Environ. Sci. Technol.*, 51, 2611-2620,
382 <https://doi.org/10.1021/acs.est.6b06151>, 2017.

383 Freedman, M. A., Hasenkopf, C. A., Beaver, M. R., and Tolbert, M. A.: Optical properties of internally mixed aerosol particles
384 composed of dicarboxylic acids and ammonium sulfate, *J. Phys. Chem. A*, 113, 13584-13592,
385 <https://doi.org/10.1021/jp906240y>, 2009.

386 Freedman, M. A.: Phase separation in organic aerosol, *Chem. Soc. Rev.*, 46, 7694-7705, <http://doi.org/10.1039/C6CS00783J>,
387 2017.

388 Freedman, M. A.: Liquid-liquid phase separation in supermicrometer and submicrometer aerosol particles, *Acc. Chem. Res.*,
389 53, 1102-1110, <https://doi.org/10.1021/acs.accounts.0c00093>, 2020.

390 Gong, Z. Y., Pan, Y. L., Videen, G., and Wang, C. J.: Optical trapping and manipulation of single particles in air: principles,
391 technical details, and applications, *J. Quant. Spectrosc. Ra.*, 214, 94-119, <https://doi.org/10.1016/j.jqsrt.2018.04.027>,
392 2018.

393 Gorkowski, K., Donahue, N. M., and Sullivan, R. C.: Emulsified and liquid-liquid phase-separated states of alpha-pinene
394 secondary organic aerosol determined using aerosol optical tweezers, *Environ. Sci. Technol.*, 51, 12154-12163,
395 <https://doi.org/10.1021/acs.est.7b03250>, 2017.

396 Gorkowski, K., Donahue, N. M., and Sullivan, R. C.: Aerosol optical tweezers constrain the morphology evolution of liquid-
397 liquid phase-separated atmospheric particles, *Chem*, 6, 204-220, <https://doi.org/10.1016/j.chempr.2019.10.018>, 2020.

398 Guo, H., Liu, J., Froyd, K. D., Roberts, J. M., Veres, P. R., Hayes, P. L., Jimenez, J. L., Nenes, A., and Weber, R. J.: Fine
399 particle pH and gas-particle phase partitioning of inorganic species in Pasadena, California, during the 2010 CalNex
400 campaign, *Atmos. Chem. Phys.*, 17, 5703-5719, <https://doi.org/10.5194/acp-17-5703-2017>, 2017.

401 Kucinski, T. M., Dawson, J. N., and Freedman, M. A.: Size-Dependent Liquid-Liquid Phase Separation in Atmospherically
402 Relevant Complex Systems, *J. Phys. Chem. Lett.*, 10, 6915-6920, <https://doi.org/10.1021/acs.jpcclett.9b02532>, 2019.

403 Kucinski, T. M., Ott, E.-J. E., and Freedman, M. A.: Flash Freeze Flow Tube to Vitrify Aerosol Particles at Fixed Relative
404 Humidity Values, *Anal. Chem.*, 92, 5207-5213, <https://doi.org/10.1021/acs.analchem.9b05757>, 2020.

405 Kucinski, T. M., Ott, E. E., and Freedman, M. A.: Dynamics of liquid-liquid phase separation in submicrometer aerosol, *J.*
406 *Phys. Chem. A*, 125, 4446-4453, <https://doi.org/10.1021/acs.jpca.1c01985>, 2021.

407 Lam, H. K., Xu, R., Choczynski, J., Davies, J. F., Ham, D., Song, M., Zuend, A., Li, W., Tse, Y. L. S., and Chan, M. N.:
408 Effects of liquid-liquid phase separation and relative humidity on the heterogeneous OH oxidation of inorganic-organic
409 aerosols: insights from methylglutaric acid and ammonium sulfate particles, *Atmos. Chem. Phys.*, 21, 2053-2066,
410 <https://doi.org/10.5194/acp-21-2053-2021>, 2021.

411 Li, M., Kan, Y., Su, H., Pöschl, U., Parekh, S. H., Bonn, M., and Cheng, Y. F.: Spatial homogeneity of pH in aerosol
412 microdroplets, *Chem*, in press, <https://doi.org/10.1016/j.chempr.2023.02.019>, 2023.

413 Lin, H. B., Eversole, J. D., and Campillo, A. J.: Continuous-wave stimulated Raman scattering in microdroplets, *P. Opt. Lett.*,
414 17, 828-830, <https://doi.org/10.1364/ol.17.000828>, 1992.

415 Losey, D. J., Parker, R. G., and Freedman, M. A.: pH Dependence of Liquid-Liquid Phase Separation in Organic Aerosol, *The*
416 *Journal of Physical Chemistry Letters*, 7, 3861-3865, [10.1021/acs.jpcclett.6b01621](https://doi.org/10.1021/acs.jpcclett.6b01621), 2016.

417 Losey, D. J., Ott, E. J. E., and Freedman, M. A.: Effects of high acidity on phase transitions of an organic aerosol, *J. Phys.*
418 *Chem. A*, 122, 3819-3828, <https://doi.org/10.1021/acs.jpca.8b00399>, 2018.

419 Ma, S. S., Chen, Z., Pang, S. F., and Zhang, Y. H.: Observations on hygroscopic growth and phase transitions of mixed 1, 2,
420 6-hexanetriol/(NH₄)₂SO₄ particles: investigation of the liquid-liquid phase separation (LLPS) dynamic process and
421 mechanism and secondary LLPS during the dehumidification, *Atmos. Chem. Phys.*, 21, 9705-9717,
422 <https://doi.org/10.5194/acp-21-9705-2021>, 2021.

423 Mahrt, F., Newman, E., Huang, Y., Ammann, M., and Bertram, A. K.: Phase behavior of hydrocarbon-like primary organic
424 aerosol and secondary organic aerosol proxies based on their elemental oxygen-to-carbon ratio, *Environ. Sci. Technol.*,
425 55, 12202-12214, <https://doi.org/10.1021/acs.est.1c02697>, 2021.

426 Mikhailov, E. F., Pöhlker, M. L., Reinmuth-Selzle, K., Vlasenko, S. S., Krüger, O. O., Fröhlich-Nowoisky, J., Pöhlker, C.,
427 Ivanova, O. A., Kiselev, A. A., Kremper, L. A., and Pöschl, U.: Water uptake of subpollen aerosol particles: hygroscopic
428 growth, cloud condensation nuclei activation, and liquid-liquid phase separation, *Atmos. Chem. Phys.*, 21, 6999-7022,
429 <https://doi.org/10.5194/acp-21-6999-2021>, 2021.

430 Mitchem, L., Buajareern, J., Ward, A. D., and Reid, J. P.: A strategy for characterizing the mixing state of immiscible aerosol
431 components and the formation of multiphase aerosol particles through coagulation, *J. Phys. Chem. B*, 110, 13700-13703,
432 <https://doi.org/10.1021/jp062874z>, 2006.

433 O'Brien, R. E., Wang, B. B., Kelly, S. T., Lundt, N., You, Y., Bertram, A. K., Leone, S. R., Laskin, A., and Gilles, M. K.:
434 Liquid-liquid phase separation in aerosol particles: imaging at the nanometer scale, *Environ. Sci. Technol.*, 49, 4995-
435 5002, <https://doi.org/10.1021/acs.est.5b00062>, 2015.

436 O'Haver, T. C.: A pragmatic introduction to signal processing with applications in scientific measurement, Kindle Direct
437 Publishing, ISBN: 9798611266687, 2022.

438 Ohno, P. E., Qin, Y., Ye, J., Wang, J., Bertram, A. K., and Martin, S. T.: Fluorescence aerosol flow tube spectroscopy to detect
439 liquid-liquid phase separation, *ACS Earth Space Chem.*, 5, 1223-1232,
440 <http://doi.org/10.1021/acsearthspacechem.1c00061>, 2021.

441 Ott, E.-J. E., Tackman, E. C., and Freedman, M. A.: Effects of Sucrose on Phase Transitions of Organic/Inorganic Aerosols,
442 *ACS Earth Space Chem.*, 4, 591-601, <http://doi.org/10.1021/acsearthspacechem.0c00006>, 2020.

443 Petters, M. D. and Kreidenweis, S. M.: A single parameter representation of hygroscopic growth and cloud condensation
444 nucleus activity, *Atmos. Chem. Phys.*, 7, 1961-1971, <https://doi.org/10.5194/acp-7-1961-2007>, 2007.

445 Preston, T. C. and Reid, J. P.: Accurate and efficient determination of the radius, refractive index, and dispersion of weakly
446 absorbing spherical particle using whispering gallery modes, *J. Opt. Soc. Am. B*, 30, 2113-2122,
447 <https://doi.org/10.1364/JOSAB.30.002113>, 2013.

448 Preston, T. C. and Reid, J. P.: Determining the size and refractive index of microspheres using the mode assignments from
449 Mie resonances, *J. Opt. Soc. Am. A*, 32, 2210-2217, <https://doi.org/10.1364/JOSAA.32.002210>, 2015.

450 Pye, H. O. T., Nenes, A., Alexander, B., Ault, A. P., Barth, M. C., Clegg, S. L., Collett, J. L., Jr., Fahey, K. M., Hennigan, C.
451 J., Herrmann, H., Kanakidou, M., Kelly, J. T., Ku, I. T., McNeill, V. F., Riemer, N., Schaefer, T., Shi, G., Tilgner, A.,
452 Walker, J. T., Wang, T., Weber, R., Xing, J., Zaveri, R. A., and Zuend, A.: The acidity of atmospheric particles and clouds,
453 *Atmos. Chem. Phys.*, 20, 4809-4888, <https://doi.org/10.5194/acp-20-4809-2020>, 2020.

454 Rafferty, A., Vennes, B., Bain, A., and Preston, T. C.: Optical trapping and light scattering in atmospheric aerosol science,
455 *Phys. Chem. Chem. Phys.*, 25, 7066-7089, <https://doi.org/10.1039/d2cp05301b>, 2023.

456 Redding, B., Schwab, M. J., and Pan, Y. L.: Raman spectroscopy of optically trapped single biological micro-particles, *Sensors*,
457 15, 19021-19046, <https://doi.org/10.3390/s150819021>, 2015.

458 Reid, J. P., Dennis-Smith, B. J., Kwamena, N. O. A., Miles, R. E. H., Hanford, K. L., and Homer, C. J.: The morphology of
459 aerosol particles consisting of hydrophobic and hydrophilic phases: hydrocarbons, alcohols and fatty acids as the
460 hydrophobic component, *Phys. Chem. Chem. Phys.*, 13, 15559-15572, <https://doi.org/10.1039/c1cp21510h>, 2011.

461 Rosenfeld, D., Sherwood, S., Wood, R., and Donner, L.: Climate effects of aerosol-cloud interactions, *Science*, 343, 379-380,
462 <https://doi.org/10.1126/science.1247490>, 2014.

463 Song, M., Marcolli, C., Krieger, U. K., Zuend, A., and Peter, T.: Liquid-liquid phase separation in aerosol particles: dependence
464 on O:C, organic functionalities, and compositional complexity, *Geophys. Res. Lett.*, 39, L19801,
465 <https://doi.org/10.1029/2012GL052807>, 2012.

466 Song, M. J., Marcolli, C., Krieger, U. K., Lienhard, D. M., and Peter, T.: Morphologies of mixed organic/inorganic/aqueous
467 aerosol droplets, *Faraday Discuss.*, 165, 289-316, <https://doi.org/10.1039/c3fd00049d>, 2013.

468 Stewart, D. J., Cai, C., Nayler, J., Preston, T. C., Reid, J. P., Krieger, U. K., Marcolli, C., and Zhang, Y. H.: Liquid-liquid
469 phase separation in mixed organic/inorganic single aqueous aerosol droplets, *J. Phys. Chem. A.*, 119, 4177-4190,
470 <https://doi.org/10.1021/acs.jpca.5b01658>, 2015.

471 Sullivan, R. C., Boyer-Chelmo, H., Gorkowski, K., and Beydoun, H.: Aerosol Optical Tweezers Elucidate the Chemistry,
472 Acidity, Phase Separations, and Morphology of Atmospheric Microdroplets, *Acc. Chem. Res.*, 11, 2498–2509,
473 <https://doi.org/10.1021/acs.accounts.0c00407>, 2020.

474 Tilgner, A., Schaefer, T., Alexander, B., Barth, M., Collett, J. L., Fahey, K. M., Nenes, A., Pye, H. O. T., Herrmann, H., and
475 McNeill, V. F.: Acidity and the multiphase chemistry of atmospheric aqueous particles and clouds, *Atmos. Chem. Phys.*,
476 21, 13483-13536, <https://doi.org/10.5194/acp-21-13483-2021>, 2021.

477 Tong, Y. K., Meng, X. X. Y., Zhou, B., Sun, R., Wu, Z. J., Hu, M., and Ye, A. P.: Detecting the pH-dependent liquid-liquid
478 phase separation of single levitated aerosol microdroplets via laser tweezers-Raman spectroscopy, *Front. Phys.*, 10,
479 <https://doi.org/10.3389/fphy.2022.969921>, 2022.

480 Wade, L. G. and Simek, J. W.: Acidity of alcohols and phenols, in: *Organic Chemistry*,
481 <https://chem.libretexts.org/@go/page/45234>, 2020.

482 Wang, M., Zheng, N., Zhao, D., Shang, J., and Zhu, T.: Using micro-Raman spectroscopy to investigate chemical composition,
483 mixing states, and heterogeneous reactions of individual atmospheric particles, *Environ. Sci. Technol.*, 55, 10243-10254,
484 <https://doi.org/10.1021/acs.est.1c01242>, 2021.

485 Weber, R. J., Guo, H. Y., Russell, A. G., and Nenes, A.: High aerosol acidity despite declining atmospheric sulfate
486 concentrations over the past 15 years, *Nat. Geosci.*, 9, 282-285, <https://doi.org/10.1038/ngeo2665>, 2016.

487 You, Y., Renbaum-Wolff, L., and Bertram, A. K.: Liquid-liquid phase separation in particles containing organics mixed with
488 ammonium sulfate, ammonium bisulfate, ammonium nitrate or sodium chloride, *Atmos. Chem. Phys.*, 13, 11723-11734,
489 <https://doi.org/10.5194/acp-13-11723-2013>, 2013.

490 You, Y., Smith, M. L., Song, M., Martin, S. T., Bertram, A. K.: Liquid-liquid phase separation in atmospherically relevant
491 particles consisting of organic species and inorganic salts, *Int. Rev. Phys. Chem.*, 33 (1), 43–77,
492 <http://doi.org/10.1080/0144235X.2014.890786>, 2014.

493 Young, A. H., Keene, W. C., Pszenny, A. A. P., Sander, R., Thornton, J. A., Riedel, T. P., and Maben, J. R.: Phase partitioning
494 of soluble trace gases with size-resolved aerosols in near-surface continental air over northern Colorado, USA, during
495 winter, *J. Geophys. Res.: Atmospheres*, 118, 9414-9427, <https://doi.org/10.1002/jgrd.50655>, 2013.

496 Zheng, G., Su, H., Wang, S., Andreae, M., Pöschl, U., and Cheng, Y.: Multiphase buffer theory explains contrasts in
497 atmospheric aerosol acidity, *Science*, 369, 1374-1377, <https://doi.org/10.1126/science.aba3719>, 2020.

498 Zhou, Q., Pang, S.-F., Wang, Y., Ma, J.-B., and Zhang, Y.-H.: Confocal Raman studies of the evolution of the physical state
499 of mixed phthalic acid/ammonium sulfate aerosol droplets and the effect of substrates, *J. Phys. Chem. B*, 118, 6198-6205,
500 <https://doi.org/10.1021/jp5004598>, 2014.